sustainability

MDPI

Article

Mechanical Behaviors and Precursory Characteristics of Coal-Burst in Deep Coal Mining for Safety-Sustainable Operations: Insights from Experimental Analysis

Xiaoran Wang [1], Jinhua Wang [2,3,*], Xin Zhou [2,3,*], Xiaofei Liu [2,3] and Shuxin Liu [2,3]

[1] State Key Laboratory for Fine Exploration and Intelligent Development of Coal Resources, China University of Mining and Technology, Xuzhou 221116, China; xrwang1992@cumt.edu.cn
[2] School of Safety Engineering, China University of Mining and Technology, Xuzhou 221116, China; liuxiaofei_1981@163.com (X.L.); liushuxin@cumt.edu.cn (S.L.)
[3] Key Laboratory of Gas and Fire Control for Coal Mines, Ministry of Education, Xuzhou 221116, China
* Correspondence: wangjinhua2023@cumt.edu.cn (J.W.); zx2020@cumt.edu.cn (X.Z.)

Abstract: Coalburst, a frequent and severe dynamic disaster, poses significant challenges to the safety and sustainable development of coal mines during deep excavation. To investigate the mechanical behaviors and precursory characteristics of coalburst subjected to in situ stress conditions, multiaxial cyclic loading experiments were conducted on cubic coal specimens, and the effects of different confining pressures on the mechanical parameters and energy evolution were analyzed. Acoustic emission (AE) technology was utilized to study the accumulation process of stress-induced damage and identify the source modes of microcracks. Then, nonlinear fractal theory and critical slowing theory were used to investigate the time-varying precursory characteristics of catastrophic failure in coalburst. The results show that as the confining pressure increases, the coal samples exhibit higher levels of elastic strain energy and dissipative energy, indicating an enhancement of plasticity. The AE count and accumulated energy show a strong correlation with cyclic loads. With an increasing number of cycles, the AE Felicity ratio gradually decreases, indicating a progressive increase in irreversible damage. Shear-mode microcracks also become more prominent with applied stress and confining pressures, as supported by varying AF/RA values of AE signals. The AE signals also follow the Hurst statistical law, and increasing applied stress and confining pressure strengthen this statistical pattern with a higher Hurst index. Throughout the cyclic loading process, certain AE varying trends were observed: the autocorrelation coefficient increased, the fractal dimension gradually decreased, and the variance suddenly increased. These trends serve as early, middle, and short–imminent warning signals, respectively, for the catastrophic failure of the loaded coal sample. These research findings contribute to a deeper understanding of coal failure evolution and provide a basis for early detection and warning of coalburst disasters, which are also essential for promoting the safe and sustainable development of deep coal mining operations.

Keywords: coalburst disaster; in-site mining cyclic loads; energy evolution; AE varying characteristics; early warning precursor; safe and sustainable mining

Citation: Wang, X.; Wang, J.; Zhou, X.; Liu, X.; Liu, S. Mechanical Behaviors and Precursory Characteristics of Coal-Burst in Deep Coal Mining for Safety-Sustainable Operations: Insights from Experimental Analysis. *Sustainability* **2024**, *16*, 2103. https://doi.org/10.3390/su16052103

Academic Editor: Pengjiao Jia

Received: 26 January 2024
Revised: 22 February 2024
Accepted: 29 February 2024
Published: 3 March 2024

1. Introduction

With the depletion of shallow resources, there is a growing trend to extract resources from deeper layers of the Earth [1,2]. However, deep mining poses challenges due to the coupling of complex stope structures and geostress, including high static confining pressure and cyclic disturbance loads caused by mining activities such as blasting, drilling, coal cutting, and periodic roof pressurization, among others [3–5]. This leads to a significant increase in the frequency and intensity of catastrophic coalburst disasters [6], ultimately limiting the safety and sustainable development of coal mines. Coalburst accidents are often accompanied by severe damage, which can instantaneously destroy working faces or

roadways of several meters to hundreds of meters, resulting in support failure, equipment damage and casualties. By the end of February 2023, a total of 159 coalbursts occurred in mines with a buried depth of more than 600 m in China [7]. For example, the coalburst accident in Longyun Coal Industry in Heze City, Shandong Province, in October 2018 caused a total of 21 deaths and significant economic losses, causing serious damage to nearly 200 m roadways. In addition, the phenomenon of coalburst in Poland, the United States, Germany, South Africa, India and dozens of other countries and regions have occurred. To accurately simulate the real stress environment of mine sites, it is crucial to conduct experiments involving the deformation and failure of coal samples under multiaxial cyclic loading and unloading while subjecting them to various confining pressures. By conducting a comprehensive analysis of the mechanical behavior and forewarning characteristics of coal under in-site mining conditions, this research can effectively uncover the failure mechanisms and precursor responses of coalburst disasters, which is crucial in promoting the safe and sustainable development of deep coal mining.

Triaxial tests have been extensively employed in the investigation of deformation, failure, and mechanical behavior of coal or rock, allowing for the replication of complex stress conditions encountered in the field [8,9]. For example, Zhou et al. [10] conducted a study on the failure characteristics and mechanisms of coal under different confining pressures and graded loads. Their findings indicated that higher confining pressures resulted in the accumulation of more elastic strain energy in the coal prior to failure. Li et al. [11] proposed the concept of an energy dissipation ratio to examine the influence of confining pressure on the mechanical properties and damage evolution of rock structures using triaxial cyclic load experiments. Du et al. discovered that the ultimate strength and residual strength of coal samples exhibited a linear increase with confining pressure, and that confining pressure could impede crack expansion while enhancing the energy storage capacity of coal [12]. Duan et al. [13] investigated the effect of triaxial cyclic disturbance on the mechanical characteristics of coal and determined that the intermediate principal stress grading cycle had a more significant influence on the intermediate and minimum principal strains compared to the maximum principal strain.

The subsequent release of stored strain energy in loaded materials, in the form of elastic waves, is referred to as acoustic emission (AE) [14,15]. By analyzing the temporal variations in AE characteristic parameters, such as ring count, energy, RA/AF value, frequency, among others, the microcracking evolution during the failure process of coal can be monitored, thereby providing an early warning for material instability precursors [16]. Li et al. conducted an analysis on the fractal characteristics of AE signals in coal samples subjected to triaxial multi-stage loading. They observed that the fractal dimension gradually decreased after the initial fluctuations in the loading stage, reaching its minimum when damage occurred [17]. Applying the critical slowing-down theory, Kong et al. [18] found that it is easier to identify the variance mutation point in the AE signal prior to coal sample failure compared to the autocorrelation coefficient. In their research, Zhou et al. [19] explored the correlation between AE parameters of coal samples and disturbance amplitude. They determined that shear cracking played a significant role in the instability and failure of loaded coal. Wang et al. established a relationship between coal sample deformation and AE response by analyzing changes in stress, strain, time, and AE parameters [20].

Indeed, the previously conducted research has contributed significantly to our understanding of the failure process and AE response characteristics of coal and rock under triaxial stress. However, further studies are needed to investigate the mechanical behavior of coal under multiaxial cyclic loads with varying confining pressures, as well as the precursor law of AE response leading up to damage and failure. The mechanism behind the instability and failure of coalburst under such in-site mining cyclic loads subjected to different confining pressures remains unclear.

To address this research gap, this paper conducted multiaxial cyclic loading and unloading failure experiments on coal samples under different confining pressures (0 MPa, 5 MPa, and 10 MPa). The aim was to analyze the effect of confining pressure on the mechan-

ical properties of coal, the evolution of energy, as well as the AE time-varying characteristics during the failure process of coal. Furthermore, the nonlinear fractal theory and critical slowing theory were employed to analyze and discuss the precursor characteristics of coal sample failure under such stress conditions. The results obtained from this research will significantly contribute to a deeper understanding of the mechanical behavior and precursor patterns associated with coalburst disasters in mining environments. Furthermore, these findings will establish an experimental foundation for disaster monitoring and early warning systems, particularly for events like coalburst. Ultimately, the insights gained from this study will help enhance the safety and sustainability of deep coal mining operations.

2. Experimental System, Material and Scheme

2.1. Experimental System

The experimental systems utilized in this paper primarily consist of a multiaxial loading device and an AE monitoring system, as depicted in Figure 1. The AE monitoring system comprises an AE acquisition card, AE sensors, pre-amplifier and Rock Test for Express-8 software. This system enables real-time collection of AE parameters and facilitates the three-dimensional localization of AE events. Throughout the testing process, the triggering threshold is set to 40 dB and the sampling rate is set at 1 MSPS. To ensure effective signal reception by the AE sensors during coal failure, a special bracket is employed to securely attach the AE sensor onto the sample's surface using a thin layer of Vaseline coupler.

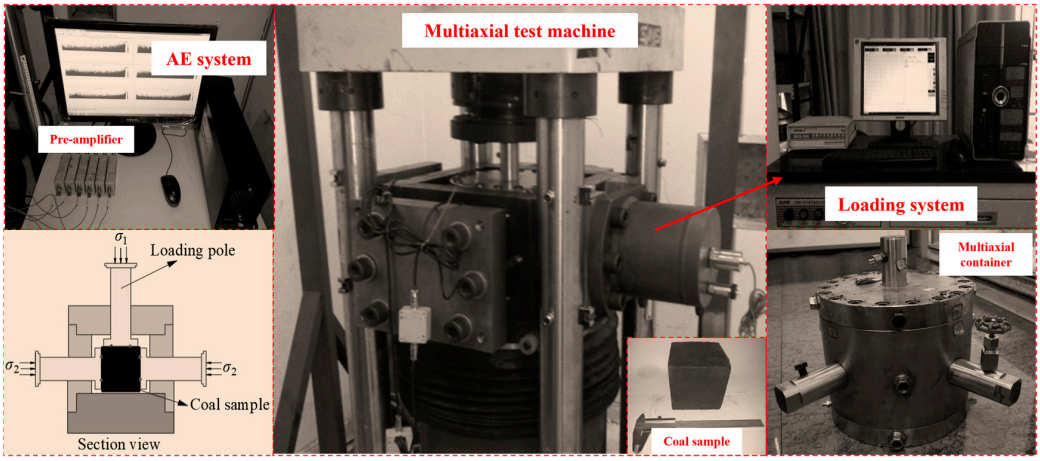

Figure 1. Experimental system and setup.

The multiaxial loading device comprises an independent axial loading and confining pressure loading system. For axial loading, the YAW4306 microcomputer-controlled electro-hydraulic servo pressure testing machine is utilized. This machine includes a hydraulic oil pump, DSC controller, and PowerTestV3.3 control program. The confining pressure loading system operates with the assistance of two hydraulic systems driving cylinders. The test force indication of these testing machines demonstrates a relative error accuracy of ±1%. The device has a maximum axial load capacity of 3000 kN and a maximum confining pressure of 30 MPa. It offers functionalities such as force or displacement closed-loop servo control and constant confining pressure retention. Additionally, the device enables real-time recording of load and displacement test curves, meeting the requirements of multiaxial cyclic loading and unloading tests under varied confining pressures.

2.2. Coal Sample Preparation and Properties

The coal samples utilized in this study was obtained from 800 m underground of a coal mine in Shanxi Province, China. To ensure sample homogeneity, the coal block was cut into cube-shaped samples measuring 100 mm × 100 mm × 100 mm using a cutting machine. A total of nine samples were prepared in this manner. The sample surfaces were

polished using a grinder to achieve a roughness of less than 0.2 mm. The basic mechanical parameters for these coal samples in the study are outlined in Table 1: density of 1.30 g/cm^3, P-wave velocity of 1383 m/s, S-wave velocity of 745 m/s, elastic modulus of 1.86 GPa, and Poisson's ratio of 0.295.

Table 1. Specimen ID of loaded coals and their mechanical parameters.

Sample ID	Density (g/cm^3)	P-Wave Velocity (m/s)	S-Wave Velocity (m/s)	Elastic Modulus (GPa)	Poisson's Ratio
C0-1	1.29	1377	742	1.79	0.297
C0-2	1.29	1389	745	1.83	0.292
C0-3	1.30	1385	743	1.89	0.297
C5-1	1.30	1382	748	1.84	0.298
C5-2	1.31	1379	749	1.87	0.296
C5-3	1.29	1390	742	1.85	0.293
C10-1	1.29	1379	745	1.92	0.295
C10-2	1.31	1378	747	1.89	0.297
C10-3	1.32	1388	744	1.86	0.289

2.3. Test Scheme and Procedure

Considering the average uniaxial compressive strength of the coal material used in this study (i.e., around 15 MPa) and the in situ three-dimensional stress state during deep coal mining ($\sigma_2 = \sigma_3 = 0.6\sim0.8\ \sigma_1$), a maximum confining pressure of 10 MPa was selected for the experiment to investigate the mechanical behaviors and precursory characteristics of coalburst under in situ stress conditions. Additionally, confining pressures of 0 MPa and 5 MPa were chosen for comparative analysis of their effects on mechanical parameters and AE response. The experimental procedure involved loading the coal sample into the test system's experimental chamber and securing it with a fixture. AE sensors were then affixed to the sample's surface, and a certain prestress was applied, ensuring close contact between the working piston and the coal sample's surface. Subsequently, all three directions of the sample were simultaneously loaded at a rate of 500 N/s. Once the lateral confining pressure ($\sigma_2 = \sigma_3$) reached the desired value, lateral loading ceased. The axial loading–unloading process then continued at a rate of 500 N/s. Unloading was halted when reaching $\sigma_1 = \sigma_2 = \sigma_3$ in each cycle, and axial loading was resumed to the predetermined stress value in the subsequent cycle. In the final cycle, the coal sample was axially loaded until it reached complete failure. Figure 2 illustrates the specific cyclic loading and unloading path.

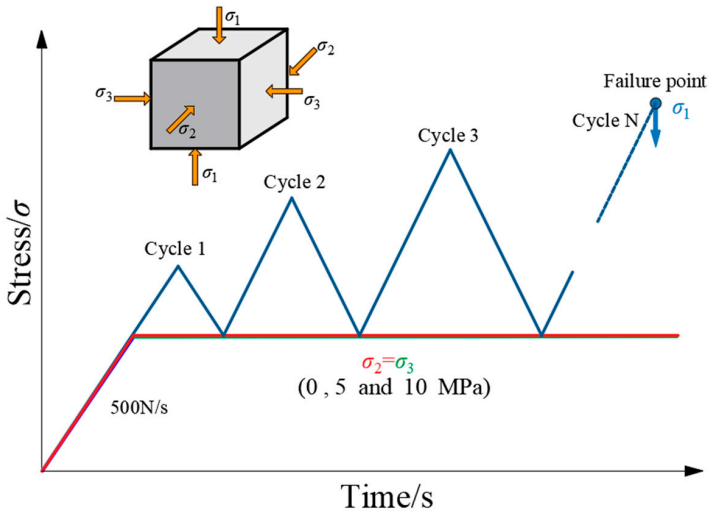

Figure 2. Stress path of the multiaxial cyclic loading procedure.

3. Mechanical and Energy Evolution of Coal under Mining Cyclic Loads

3.1. Mechanical Properties

To improve the reliability of the test results, the experiment was conducted three times at each confining pressure (0 MPa: C0-1, C0-2, and C0-3; 5 MPa: C5-1, C5-2, and C5-3; 10 MPa: C10-1, C10-2, and C10-3). Considering the repeatability and similarity of the results, only one sample at each confining pressure was analyzed and presented here. Figure 3 illustrates the mechanical curves of sample C0-1, C5-2, and C10-2 under various confining pressures, as determined from the experimental data.

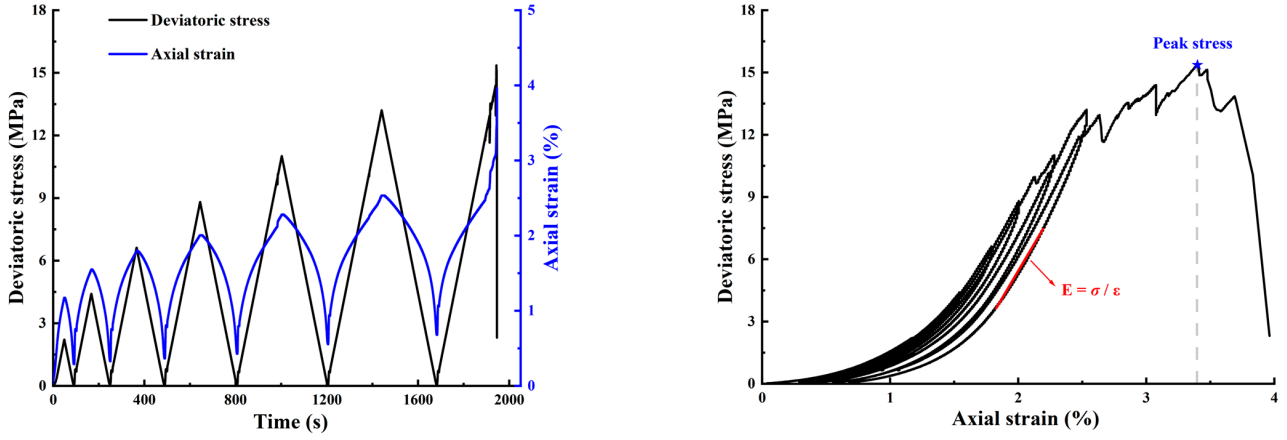

(**a**) C0-1

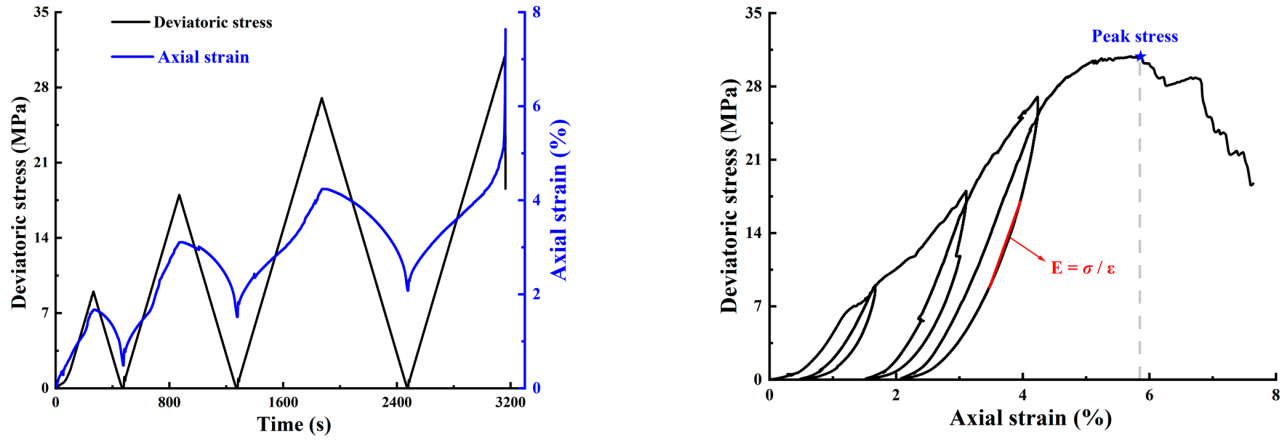

(**b**) C5-2

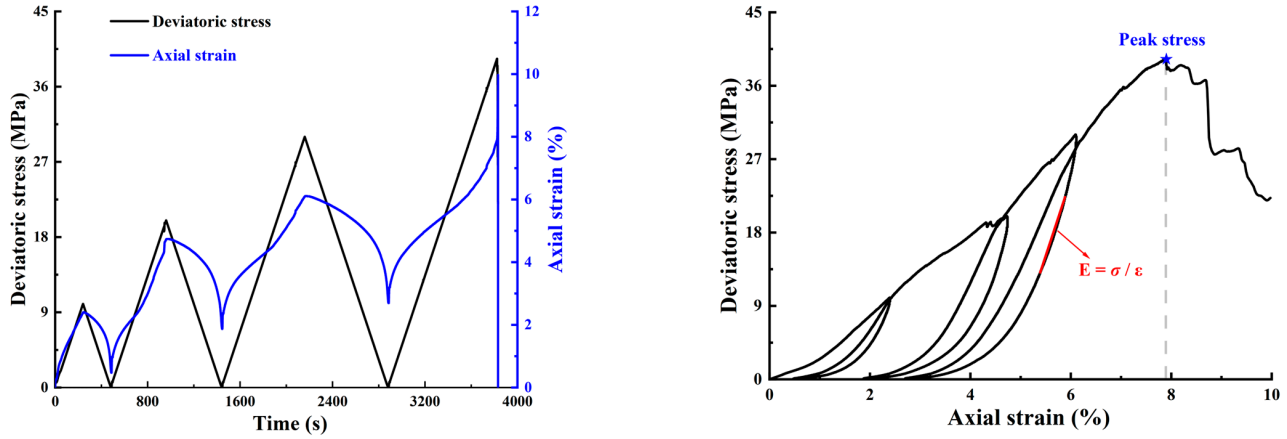

(**c**) C10-2

Figure 3. Mechanical curves of coal under multiaxial cyclic loads.

Figure 3 illustrates the mechanical curves of coal under multiaxial cyclic loading with various confining pressures, where the deviatoric represents the difference of axial stress and the confining presses (i.e., $\sigma_1 - \sigma_3$). It is evident that the deformation process of coal can be divided into four stages [21,22]: (1) Initial compaction stage: During this stage, the coal sample experiences cyclic loading, leading to the compaction of the original microcracks. The stress and strain exhibited during this stage are relatively low. (2) Linear elastic stage: This stage occurs when the specimen is loaded to around 30–60% of its strength stress. Vertical compaction continues, and internal cracks gradually expand in a stable manner, resulting in a near-linear relationship between stress and strain. (3) Plastic deformation stage: As the cyclic process continues, a significant number of new cracks are generated, and existing cracks expand rapidly. The stress and strain exhibit distinct nonlinear characteristics, and irreversible deformation rapidly increases. (4) Post-peak stage: In this stage, microcracks continue to expand and penetrate in an unstable manner. The axial stress suddenly decreases, while the axial strain experiences a sharp increase. Eventually, a macroscopic fracture surface forms, leading to complete sample failure.

In order to analyze the influence of confining pressure and cyclic numbers on the mechanical properties of coal samples, key parameters such as peak stress, peak strain, residual strain, and elastic modulus are extracted from Figure 3. These results are presented in Figure 4. The analysis reveals a significant positive linear correlation between the mechanical parameters (e.g., peak strength, peak strain, and elastic modulus) of coal samples and confining pressure. Comparatively, when subjected to higher confining pressures (5 MPa and 10 MPa) as opposed to uniaxial (i.e., confining pressure = 0 MPa) cyclic loading, the mechanical parameters of coal samples increase notably: the peak stress intensity increases by 100.91% and 156.18% (Figure 4a), the peak strain increases by 92.93% and 151.77% (Figure 4b), and the elastic modulus increases by 18.26% and 36.52%, respectively (Figure 4c). During cyclic loading of coal samples, the residual deformation in each cycle progressively increases due to the elevated stress level. Additionally, the presence of confining pressure further amplifies the residual deformation. Indeed, higher confining pressures resulted in larger residual deformation and hysteresis loops in the strain–stress curve after each cycle (Figure 4d). Moreover, the elastic modulus generally exhibits an increasing trend with an increment in the number of cycles.

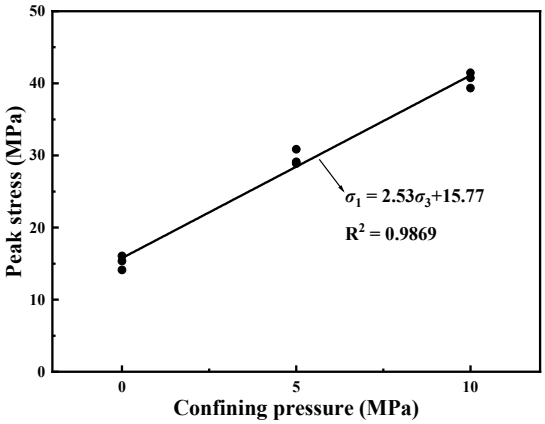

(**a**) Peak stress

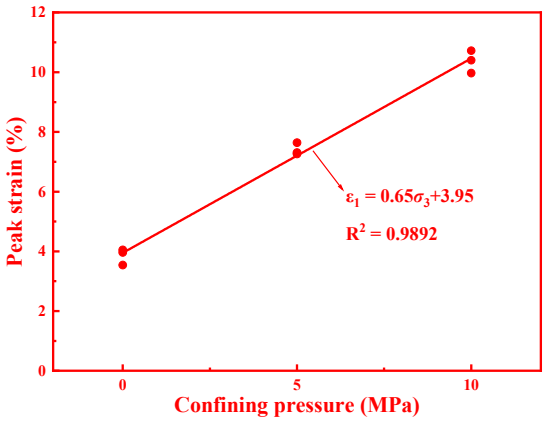

(**b**) peak strain

Figure 4. *Cont.*

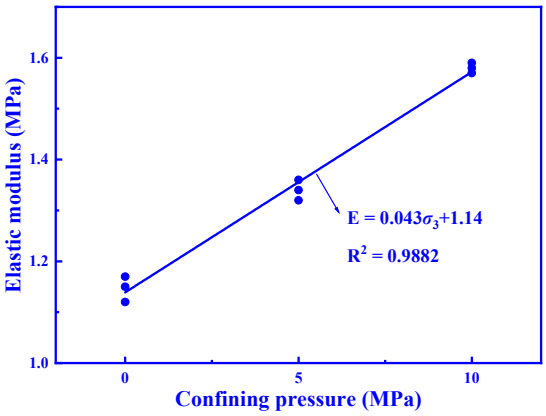

(**c**) elastic modulus

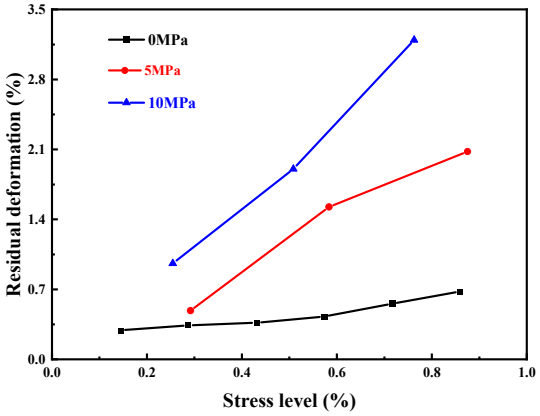

(**d**) residual deformation

Figure 4. Confining pressure effects on mechanical properties of coal.

3.2. Energy Evolution Characteristics

The deformation and failure of samples are fundamentally unstable phenomena resulting from energy transformation, which encompasses the energy accumulation, dissipation, and instantaneous release [23]. During cyclic loading and unloading, the axial stress applies positive work to compress the coal sample, causing it to store energy through elastic deformation. When unloading occurs, a portion of the stored energy is released, while the remaining energy is dissipated, leading to irreversible deformation. Assuming there is no heat exchange during the loading process, part of the total work conducted by the external world (referred to as the total input energy, U_T) is converted into reversible energy (U_R), which accumulates elastically within the coal sample. The other portion is transformed into irreversible energy (U_I), which is consumed during the fracture process of the coal sample. This energy specifically consists of the newly generated surface energy due to crack propagation, as well as the energy of geophysical signals such as AE released to the surroundings.

In the cyclic processes before the final cycle, U_R and U_I can be obtained by integrating the stress and strain curves of the loading and unloading stages separately (Figure 5a), and U_T is the sum of U_R and U_I. For the last cyclic process (Figure 5b), the following formulas are used to calculate U_T, U_R and U_I [24,25]:

$$U_T = Al\int_0^{\varepsilon_1^2} \sigma_1 d\varepsilon_1 = \frac{1}{2}Al\sum_{i=1}^{n}\left(\sigma_1^i + \sigma_1^{i-1}\right)\left(\varepsilon_1^i - \varepsilon_1^{i-1}\right) \quad (1)$$

$$U_R = Al\frac{\sigma_1^2}{2E} \quad (2)$$

$$U_I = U_T - U_R \quad (3)$$

where A and l are the area and length of the coal specimen, respectively; E is the Young's modulus.

The values of U_T, U_R, and U_I are calculated and presented in Table 2 based on Equations (1) to (3) for different confining pressures and cycles. When the confining pressure remains constant, U_R at the peak load is significantly larger than U_I in the previous cyclic process (i.e., at low stress levels), indicating that the majority of U_T is stored as reversible elastic energy. As the number of cycles increases (corresponding to higher stress levels), both U_R and U_I exhibit gradual increments; however, the increase in U_I surpasses that of U_R, leading to a gradual reduction in the disparity between U_R and U_I. During the final cyclic process, U_R stored in the sample after reaching the peak load is rapidly converted into U_I, resulting in instantaneous energy release and sample destruction. Under the influence of the confining pressure, both U_R and U_I within each cycle exceed the values observed without the confining pressure. Moreover, a higher confining pressure enables

the sample to withstand greater axial stress, thereby amplifying the conversion of U_R and U_I. The presence of the confining pressure restricts the outward ejection of the sample, inhibiting the release of U_R, enhancing the plasticity of the coal sample, weakening the dynamic impact effect, and yielding a substantial residual stress even after failure of the sample (Table 2).

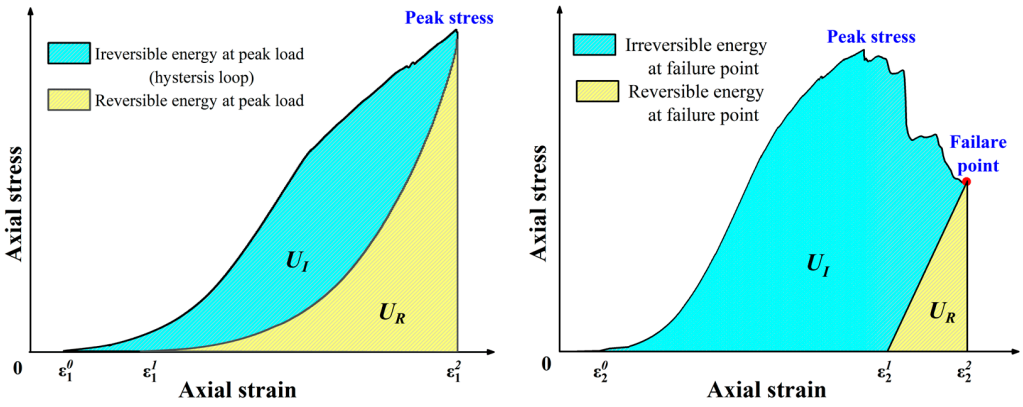

Figure 5. Illustration of energy calculation under multiaxial cyclic loads. (**a**) Cyclic processes before the final cycle; (**b**) last cyclic loading.

Table 2. Energy and AE varying results of coal under multiaxial cyclic loads.

Confining Pressure	Cycles	Residual Deformation (%)	Reversible Energy (J)	Irreversible Energy (J)	Input Energy (J)	Felicity Ratio	*D* Value
0 MPa	1	0.31	6.52	1.99	8.51	/	1.613
	2	0.33	16.23	3.55	19.78	1.532	
	3	0.38	26.96	5.79	32.75	1.203	1.554
	4	0.44	38.03	8.54	46.57	1.023	
	5	0.57	51.75	19.28	71.03	0.953	1.455
	6	0.68	66.94	22.10	89.04	0.825	
	7	/	10.07	210.18	250.85	0.715	1.397
5 MPa	1	0.49	34.64	15.14	49.78	/	1.578
	2	1.52	160.01	65.27	225.27	1.060	1.510
	3	2.08	192.87	157.73	350.60	0.894	1.456
	4	/	111.03	1052.9	1163.93	0.722	1.329
10 MPa	1	0.49	55.00	22.30	77.30	/	1.505
	2	1.91	251.97	83.04	335.01	1.102	1.429
	3	2.70	315.10	230.13	545.23	0.944	1.373
	4	/	178.36	1412.13	1590.49	0.781	1.290

4. AE Varying Characteristics of Coal under Multiaxial Cyclic Loads

4.1. Evolution of AE Characteristic Parameters

The AE characteristic parameters are capable of effectively reflecting the microcracking evolution of coal samples under different stages of mechanical loads [26]. Figure 6 illustrates the time-varying evolution of the AE count and accumulated energy of coal samples subjected to multiaxial cyclic loads. Each cycle exhibits distinct phases in the AE count, including a quiet period, pre-peak active period, peak period, and post-peak period. During the quiet period, which occurs prior to compaction and before reaching the maximum stress of the previous cycle, the occurrence of AE events is minimal. In the pre-peak active period, the AE count gradually increases as cracks start to form in the coal sample and reach the maximum stress of the previous cycle. The peak period corresponds to

the cyclic loading stress reaching its maximum value, during which the AE count also reaches its maximum. The post-peak period predominantly occurs during the unloading phase, characterized by a gradual decrease in AE counts, until no signals are detected. The accumulated AE energy progressively increases with each cycle, rising proportionally with the applied load. Conversely, during the unloading phase, the accumulated AE energy remains relatively constant. The increase in confining pressure significantly amplifies both the AE count and energy, suggesting more active microcracking behaviors in coal samples under confining pressure.

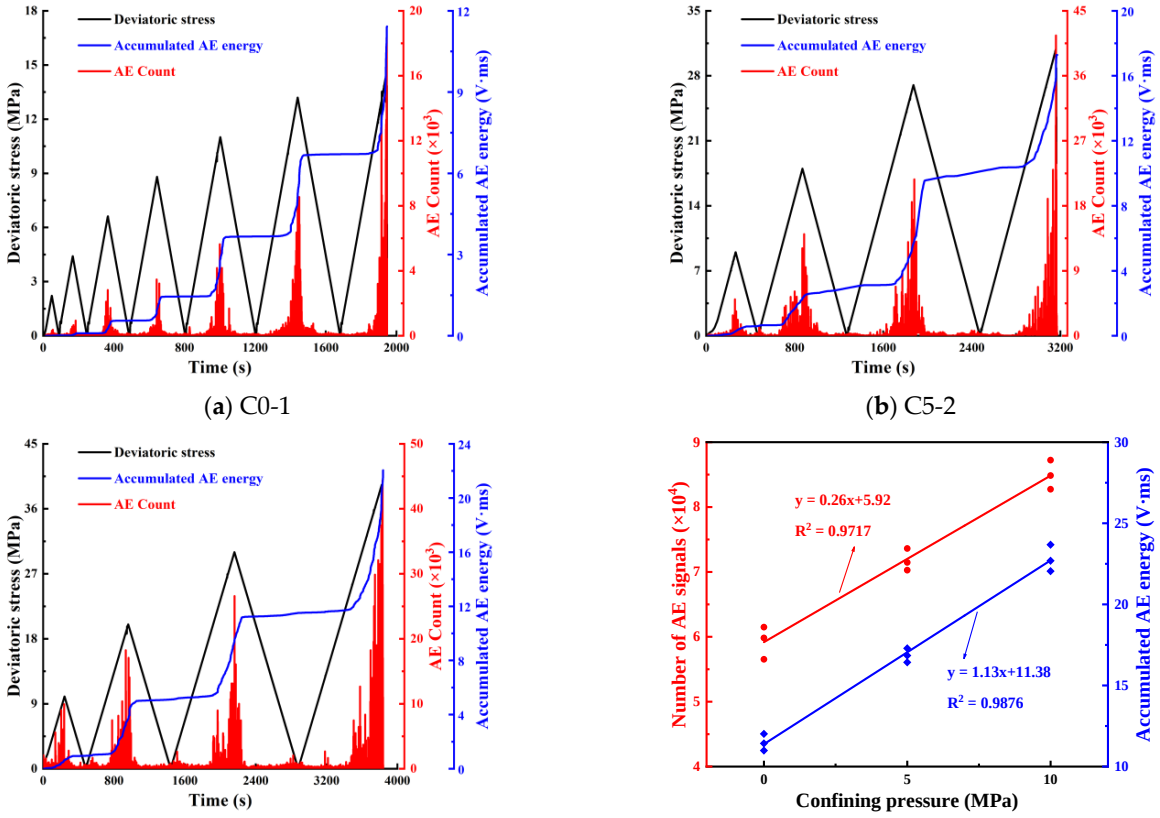

Figure 6. AE time-varying characteristics of coal under multiaxial cyclic loads.

Research has shown that when the applied load is below the maximum load ever experienced, the recorded AE signal is minimal. Conversely, when the load exceeds the maximum load ever experienced, the AE events become active and increase rapidly. This phenomenon is known as the Kaiser effect, also referred to as the memory effect [27]. The accuracy of the Kaiser effect can be evaluated using the Felicity ratio, which is defined as the ratio between the stress level at which the AE signal experiences a rapid increase and the maximum stress ever experienced [28]:

$$F_i = \frac{X_i}{X_m} \tag{4}$$

where F_i is the Felicity ratio of the i-th cycle; X_i is the stress when the AE signal increases rapidly at the i-th cycle, and X_m is the maximum stress of the previous cyclic loads.

When the Felicity ratio is equal to or greater than one, it indicates that the AE signal exhibits a significant memory effect regarding the maximum bearing stress. Conversely, a Felicity value less than one suggests an anti-Kaiser effect in the AE behavior, which indicates more severe microcracks and an increased level of damage. The severity of the damage level of the loaded material can be inferred based on the magnitude of the Felicity

ratio, with smaller values corresponding to more pronounced effects. Table 2 illustrates the AE Felicity ratios at different stages of coal under multiaxial cyclic loads. During the early stages of the whole cyclic process, the Felicity ratio is relatively large. This suggests that the coal sample's internal cracks are in the compaction stage, while the recovery of the AE signals lags behind. As the number of loading and unloading cycles increases, the Felicity ratio gradually decreases, indicating a decrease in the accuracy of the Kaiser effect memory. Comparing the Felicity ratio at each cycle reveals that as the confining pressure increases, the ratio approaches one. This suggests that the presence of confining pressure enhances the stability of the Kaiser effect memory, with higher confining pressure leading to improved stability.

4.2. Shear-Tensile Property of Microcracks Judged by AE

The acoustic emission monitoring system used in the experiment has eight channels, and we selected the data from one of the channels for analysis. Whenever the sensor picks up a waveform, we determine that the waveform is generated by a microcrack [29]. According to the waveform characteristics of the AE signals, the relative amplitude (RA) and the average frequency (AF) can provide insights into the shear-tensile properties of stress-induced microcracks. The RA is determined as the ratio of the AE rise time to the amplitude, while the AF is calculated as the ratio of the AE count to the duration [30–32]. Previous studies have indicated that shear cracks typically produce low-frequency and high-amplitude AE signals, resulting in a small AF to RA ratio. Conversely, tensile microcracks are associated with high-frequency and low-amplitude AE signals, leading to a large AF to RA ratio [30,33]. In this paper, the ratio K of AF to RA is employed to discern the tensile and shear properties of microcracks during the failure process of coal subjected to multiaxial cyclic loading conditions. A threshold value of K = 2 is used; when K > 2, it indicates a tensile crack, whereas when K < 2, it suggests a shear crack [34,35].

The probability distribution density of RA-AF for different cycles under varying confining pressures is depicted in Figure 7. The initial cyclic process indicates that AE events are predominantly concentrated in the upper left region (small RA value, large AF value, K > 2), suggesting that tensile microcracks primarily develop in the coal sample at low stress levels. As the number of cycles increases, the stress level gradually escalates, and the dense area of the AE signal progressively shifts from the upper left to the lower right (large RA value, small AF value, K < 2). This transition signifies an increase in shear microcracks within the coal sample, reaching its maximum value during the final cyclic loading phase. Moreover, the density of shear microcracks also gradually increases with higher confining pressures. This phenomenon arises due to changes in the stress state of the coal sample during the loading and unloading process. Consequently, the damage evolution process and crack formation in the coal sample are altered. The growth of shear microcracks with increasing stress and confining pressure underscores their crucial role in the failure process of coal samples under confining pressures.

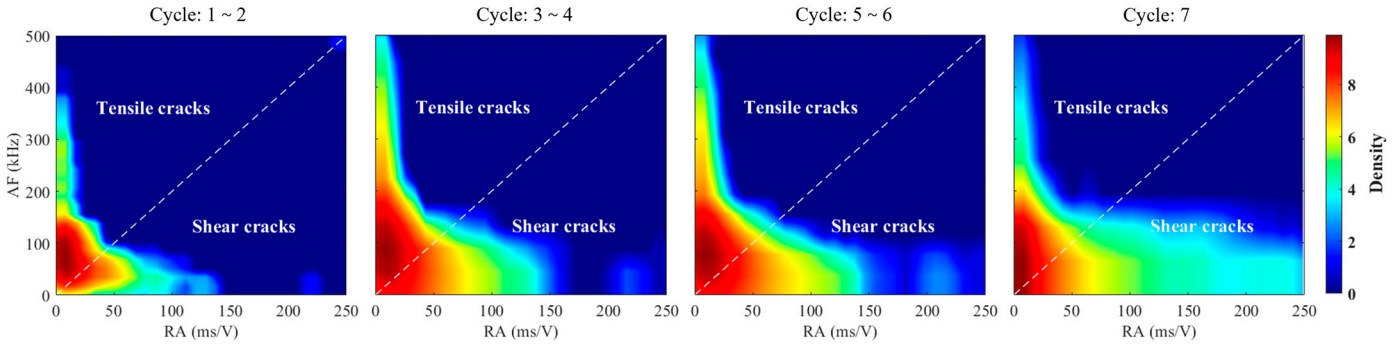

(**a**) C0-1

Figure 7. *Cont.*

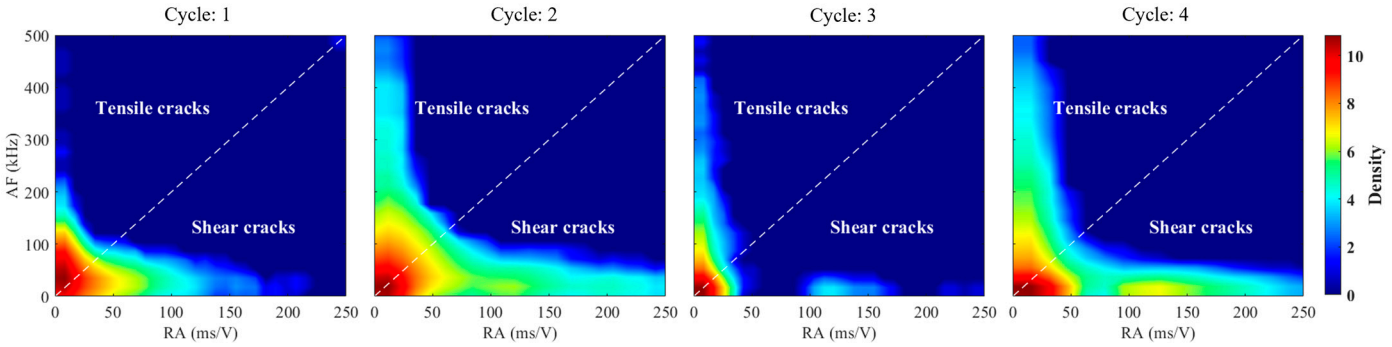

(**b**) C5-2

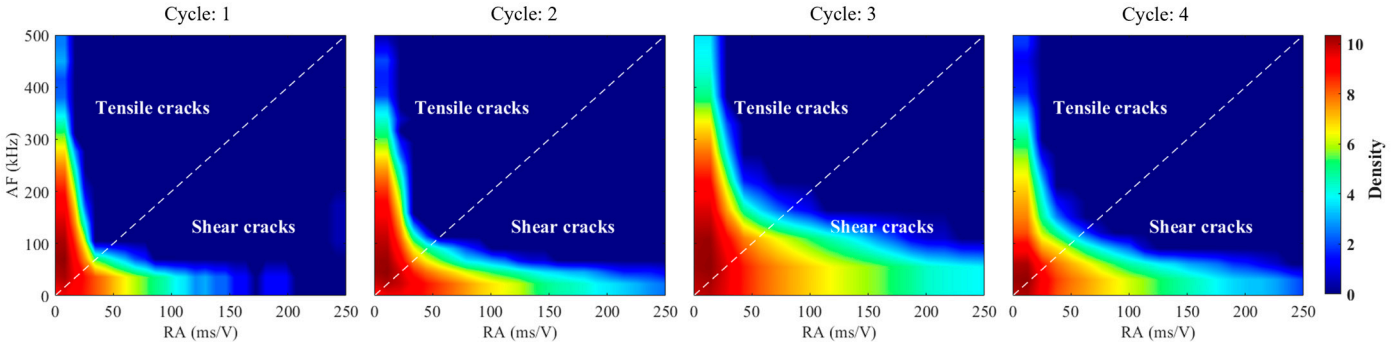

(**c**) C10-2

Figure 7. RA-AF probability density of coal under multiaxial cyclic loads.

Figure 8 presents the cumulative number of tensile and shear microcracks with respect to time, providing further insight into the evolution of these microcracks during the multiaxial cyclic process of coal samples. It is observed that, at the same confining pressures, both tensile and shear microcracks exhibit a substantial increase during the loading stage of each cycle, while their numbers remain relatively stable during the unloading stage. This behavior can be attributed to the continuous development and expansion of coal sample microcracks, as well as the generation of new microcracks and their connection during the loading process, which collectively contribute to the overall increase in microcrack numbers.

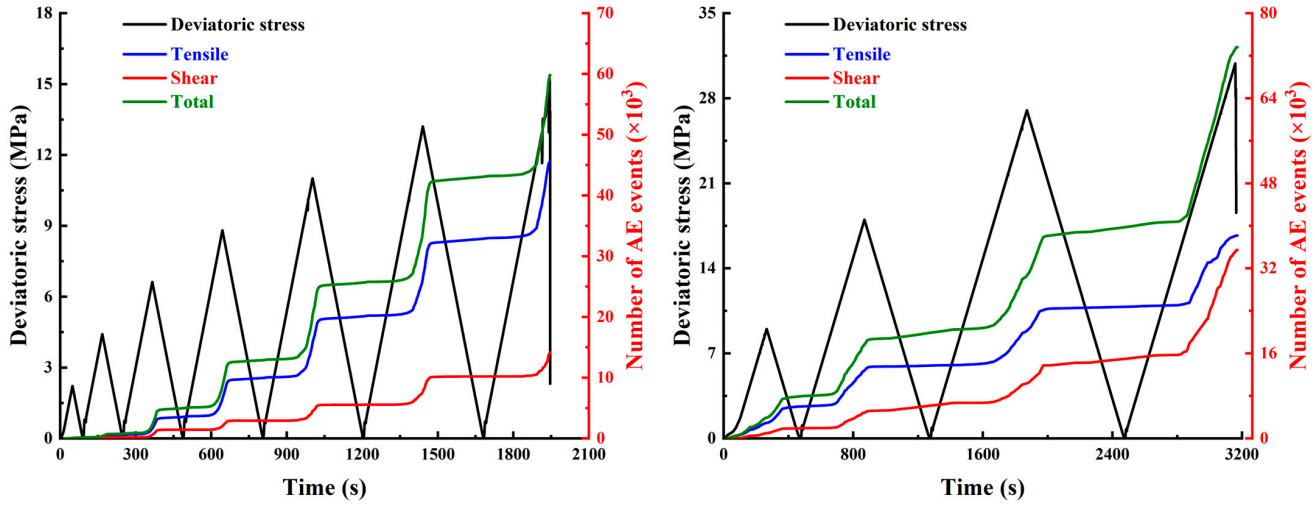

(**a**) C0-1 (**b**) C5-2

Figure 8. *Cont.*

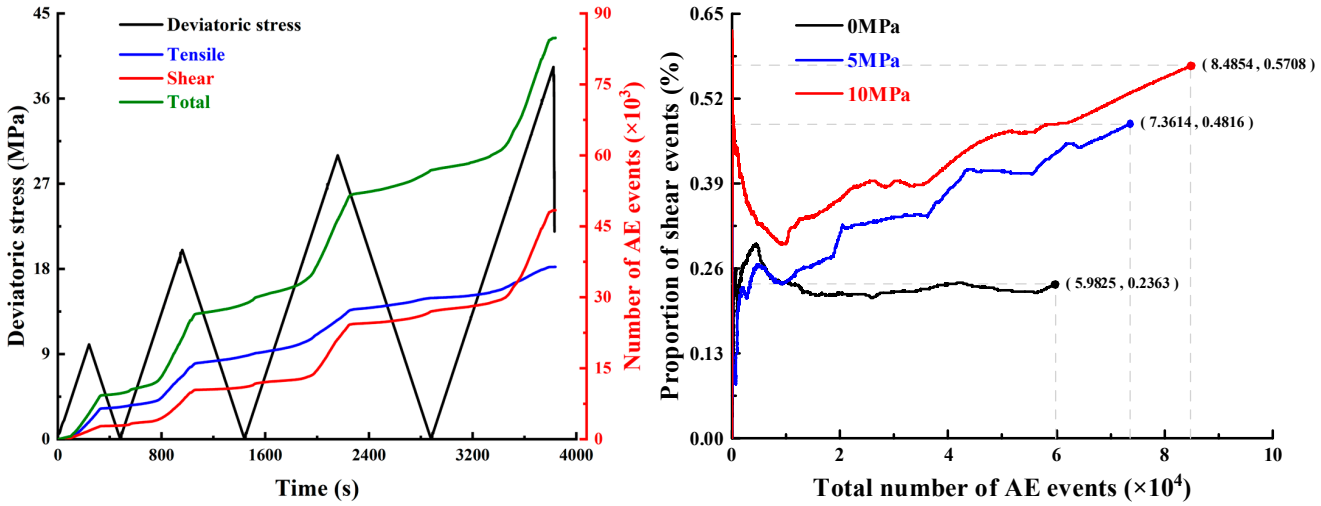

(**c**) C10-2 (**d**) confining pressure effects

Figure 8. Shear and tensile events evolution of coal under multiaxial cyclic loads.

Upon analyzing the specific confining pressures, it is evident that, at a confining pressure of 0 MPa, tensile microcracks dominate the entire cyclic process (see Figure 8a). However, under the influence of confining pressure, the microcracks generated at the initial cycles in the coal sample are still predominantly tensile cracks. Over subsequent cycles, the occurrence of shear microcracks gradually increases and ultimately becomes the dominant microcrack mechanism (Figure 8b,c). Notably, prior to the failure of the coal sample, there is a significant and abrupt rise in shear events, with a greater proportion of shear microcracks generated as the confining pressure increases (Figure 8d). This observation supports the notion that confining pressure promotes the formation of shear cracks, and the behavior of shear cracks serves as a more intuitive indicator of the coal sample failure process. These findings align with the occurrence of tensile-shear mixed failure mechanisms observed at lower confining pressures, with shear fracturing surfaces taking precedence at higher confining pressures.

4.3. RS Fractal Features of AE Signals

The temporal evolution of AE signals during the damage process of coal samples exhibits a nonlinear behavior [36] The paper selects acoustic emission counts for RS fractal analysis. Fractal theory, being a nonlinear scientific framework, has the capability to unveil identical structural principles within seemingly unrelated phenomena. The RS analysis method, initially proposed by Hurst, has found extensive utility in analyzing diverse time series [34]. In this study, the AE signal is considered as a time series $\{X(t), t = 1, 2, 3, \ldots, N\}$, comprising N subintervals of equal length A. Subsequently, for each subinterval, the following relationship holds [36]:

$$X_{t,n} = \sum_{n=1}^{A} (X_n - M_n) \tag{5}$$

where M_n represents the average value of the n-th subinterval X_n, and $X_{t,n}$ denotes the cumulative deviation of the n-th subinterval.

Hurst found that the statistical relationship between the range R of $X_{t,n}$ and the standard deviation S of the X_n sequence can be expressed in exponential form [37,38], as follows:

$$\frac{R}{S} = K(n)^H \tag{6}$$

where H represents the Hurst index, which serves as a measure of the statistical correlation within a time series. When $0 < H < 0.5$, the time series exhibits inverse state persistence,

indicating a negative correlation. Conversely, when $0.5 < H < 1$, state persistence is observed, and the time series is characterized by a trend-enhanced sequence with an overall positive correlation that is increasing.

The logarithm is applied to both sides of Equation (6). Following this, a least square regression analysis can be conducted using the variables $\log(n)$ and $\log(R/S)n$ to calculate the H value. The H value is then used to calculate the fractal dimension D.

$$D = 2 - H \tag{7}$$

The fractal dimension D is a measure of the irregularity and complexity of a time series. In the case of AE time series, a higher D value indicates a more irregular and complex deformation process, whereas a lower D value suggests a more regular deformation process. Figure 9 illustrates the variation of D values obtained from the slope of the fitted line, and Table 2 presents the calculated D values. The results show that for each cyclic loading and unloading under different confining pressures, the H values of the coal samples range between 0.5 and 1.0. This indicates a positive correlation between the microcracking behaviors in loaded coal samples and the Hurst statistical law of the AE signals. With an increasing number of cycles, the D value exhibits a declining trend overall, implying a strengthening regularity in the deformation failure of the coal samples. Comparing the D values under different confining pressures reveals a negative correlation with the confining pressure. Higher confining pressures result in smaller D values, suggesting that confining pressure enhances the regularity of deformation and failure in coal samples.

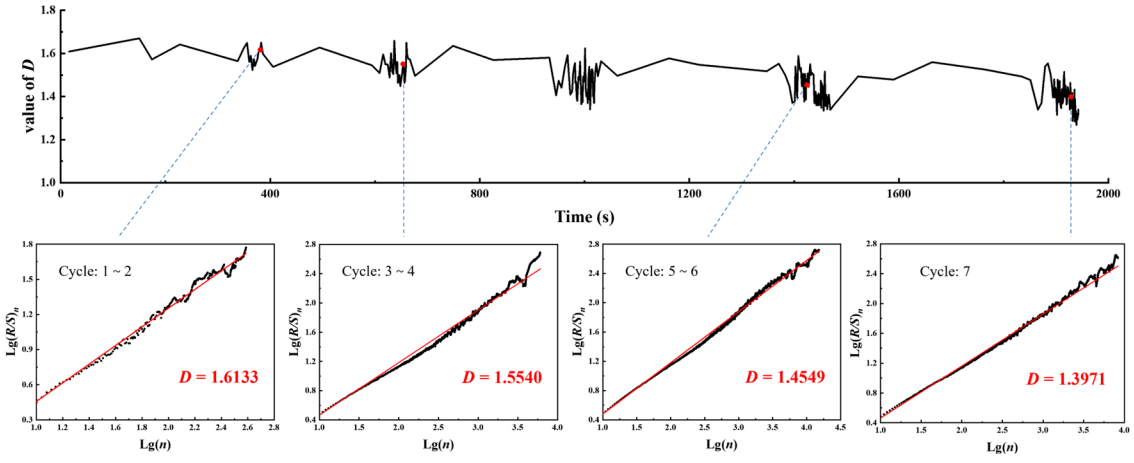

(**a**) C0-1

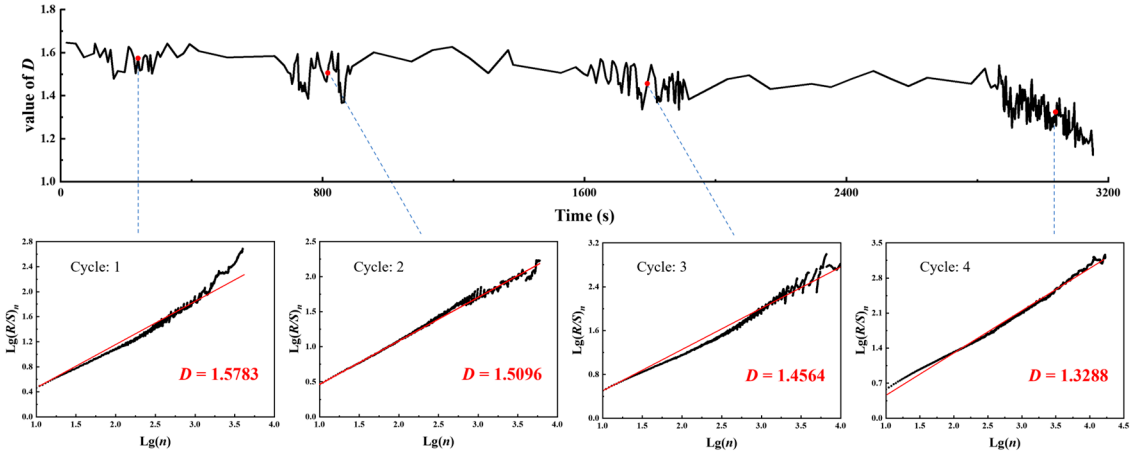

(**b**) C5-2

Figure 9. *Cont.*

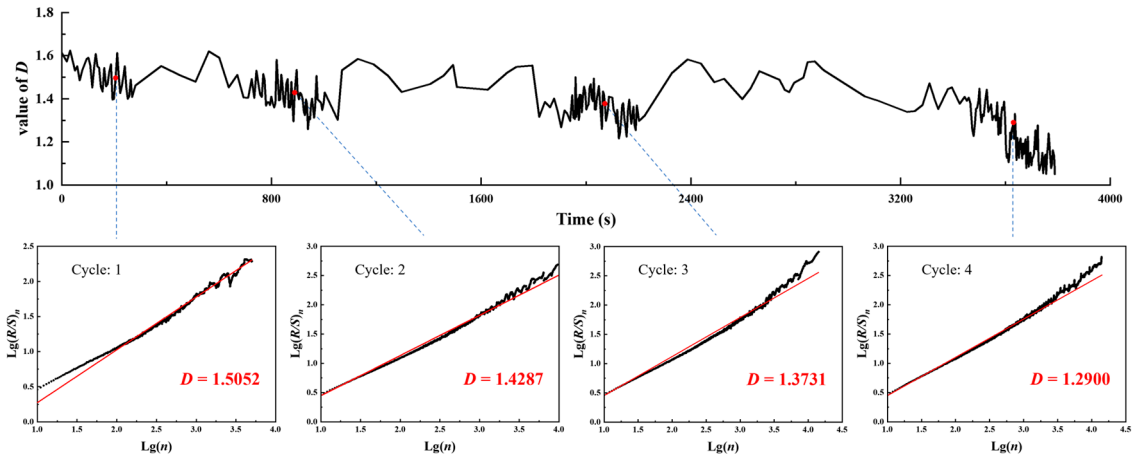

(**c**) C10-2

Figure 9. AE nonlinear fractal features of coal under multiaxial cyclic loads.

5. Discussion

5.1. Confining Pressure Effects on Coal Mechanical and AE Parameters

Based on the analysis above, it can be observed that the deformation stage of coal samples under different confining pressures exhibit similar basic characteristics. However, as the confining pressure increases, the elastic modulus, peak strength, and peak strain of the coal samples also increase. This can be attributed to the propensity of microcracks within the coal sample to deform under stress. Higher confining pressures result in the strengthening of the physical and mechanical properties of the coal samples, along with enhanced friction on the fracture surface. These factors further impede the deformation and failure of the coal samples, thereby increasing their bearing capacity. Additionally, the application of confining pressure improves the stiffness and ductility of the coal sample, leading to increased compressive strength. Consequently, the coal samples are capable of withstanding higher levels of stress, achieving greater deformation, and exhibiting more pronounced plastic characteristics. Moreover, the enhanced stiffness resulting from higher confining pressures prolongs the time required for failure to occur.

The energy conversion during a complete cycle is influenced by both axial stress and axial strain. When comparing the same axial strain, a higher confining pressure results in greater energy conversion. This is because increased confining pressure enhances interlocking friction among surrounding fractures, requiring more energy absorption and dissipation for the same level of damage. The effect of confining pressure causes a higher proportion of the external force to be converted into reversible energy in the form of elastic strain energy during the compaction stage and elastic stage. In the plastic stage, reversible energy continues to dominate, although it slows down as microcracks generate and propagate in an unstable manner, leading to an increase in irreversible, dissipative energy. During the post-peak stage, the microcracks of the coal sample experience continuous expansion and convergence, resulting in the ultimate destruction of the coal sample as a whole. This stage witnesses a significant increase in irreversible energy.

The AE count serves as a more reliable indicator of the development of microcracks in loaded coal samples. A higher AE count signifies a faster crack propagation rate. As the confining pressure increases, the AE count also tends to increase. This can be attributed to the stronger constraint effect imposed on the coal sample by higher confining pressures. The application of confining pressure enhances both the bearing capacity and shear failure strength of the coal sample. Consequently, shear failure occurs along the internal weak structural planes, and at both ends of the coal sample during cyclic loading and unloading. This phenomenon results in the generation of a larger number of shear cracks. Over time, the fracture morphology of the coal sample undergoes a gradual

transition from a predominantly tensile fracture-dominated complex form to a shear-dominated fracture morphology.

5.2. AE Multi-Parameter Precursor Response

During the transition of a complex dynamical system from one phase state to another, certain dispersed fluctuation phenomena, which promote the formation of new phases, often emerge near the critical point. These phenomena include an increase in amplitude, prolongation of fluctuation time, slow recovery rate of disturbance, and decreased recovery ability. When a system's parameter approaches a critical threshold, the phenomenon known as critical slowing-down causes an increase in the autocorrelation coefficient and variance in the system's characterization.

As a result, the variance and autocorrelation coefficient of the analysis parameter are commonly employed to observe the precursory response. These measures are used to detect the subtle changes that occur before the transition from one phase state to another. By monitoring the changes in variance and autocorrelation coefficient, researchers can gain insight into the upcoming transition in the complex dynamical system.

Let us assume the existence of a state parameter that experiences a forced disturbance with a period of Δt. During the disturbance process, the parameter's recovery rate is denoted as λ. A regression model can be formulated to approximate the relationship, which is expressed as follows [39,40]:

$$x_{n+1} = e^{\lambda \Delta t} x_n + s\varepsilon_n \tag{8}$$

where, X_n represents the deviation of the parameter from its equilibrium state. The square of S denotes the variance, which is a measure of the degree of deviation of the data from the average value. ε_n is a random variable that follows a normal distribution. When the recovery rate λ and the disturbance period Δt are independent of X_n, the regression model can be simplified as follows:

$$x_{n+1} = \alpha x_n + s\varepsilon_n \tag{9}$$

where α is the autocorrelation coefficient.

The autocorrelation coefficient α can be calculated with the formula $\alpha = e^{\lambda \Delta t}$, which relates to the exponential relationship described in Equation (8). The autocorrelation coefficient (denoted as ρ) is a statistical measure that quantifies the correlation between different moments of the same variable. Specifically, for a parameter q with a total of n data points and a lag step of j, the calculation formula for the autocorrelation coefficient is as follows:

$$\alpha = \sum_{i=1}^{n-1} \left(\frac{q_i - \overline{q}}{s} \right) \left(\frac{q_{i+j} - \overline{q}}{s} \right) \tag{10}$$

By utilizing the variance to analyze the regression process represented by Equation (9), we can obtain the following result:

$$\mathrm{Var}(x_{n+1}) = E\left(x_n^2\right) + (E(x_n))^2 = \frac{s^2}{1 - \alpha^2} \tag{11}$$

In the approach to the critical point, several behaviors become apparent. The recovery rate of disturbances slows down, the autocorrelation coefficient increases, and the variance tends towards infinity. These changes in the autocorrelation coefficient and variance of the system can serve as precursory signals of coal sample failure, as they align with the system's nearing of the critical point. Furthermore, the fractal dimension D, obtained through fractal analysis, exhibits variations throughout the loading and unloading process. Before the critical failure of the coal sample, a significant mutation in the D value occurs, making it another useful precursor signal.

Determining the appropriate window length and lag step length is essential before analyzing the autocorrelation coefficient and variance. The window length represents the

basic unit for sequence calculation, while the lag step length signifies the lag sequence length from one sequence of the selected window length to another identical new sequence. In this paper, the loading and unloading experimental data of coal samples under various confining pressures utilize a window length of 3000 and a lag step of 1500. Figure 10 displays the obtained critical diffusion characteristics and variations in the fractal dimension D for certain AE parameters under different confining pressures.

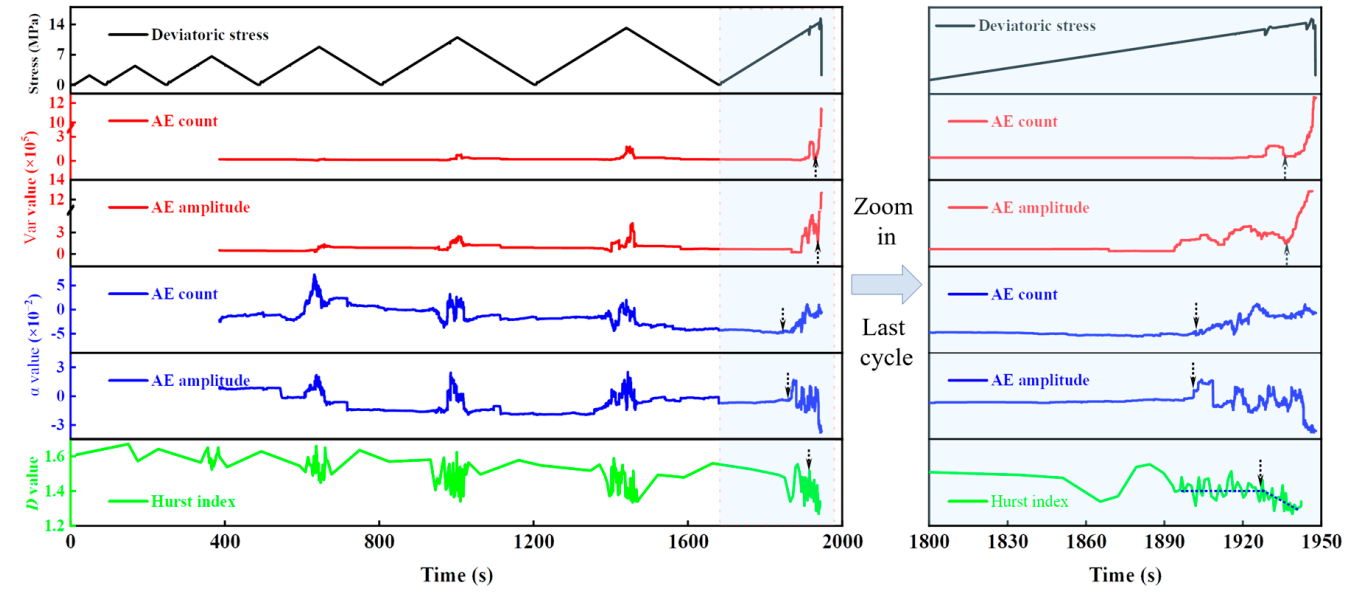

(**a**) C0-1

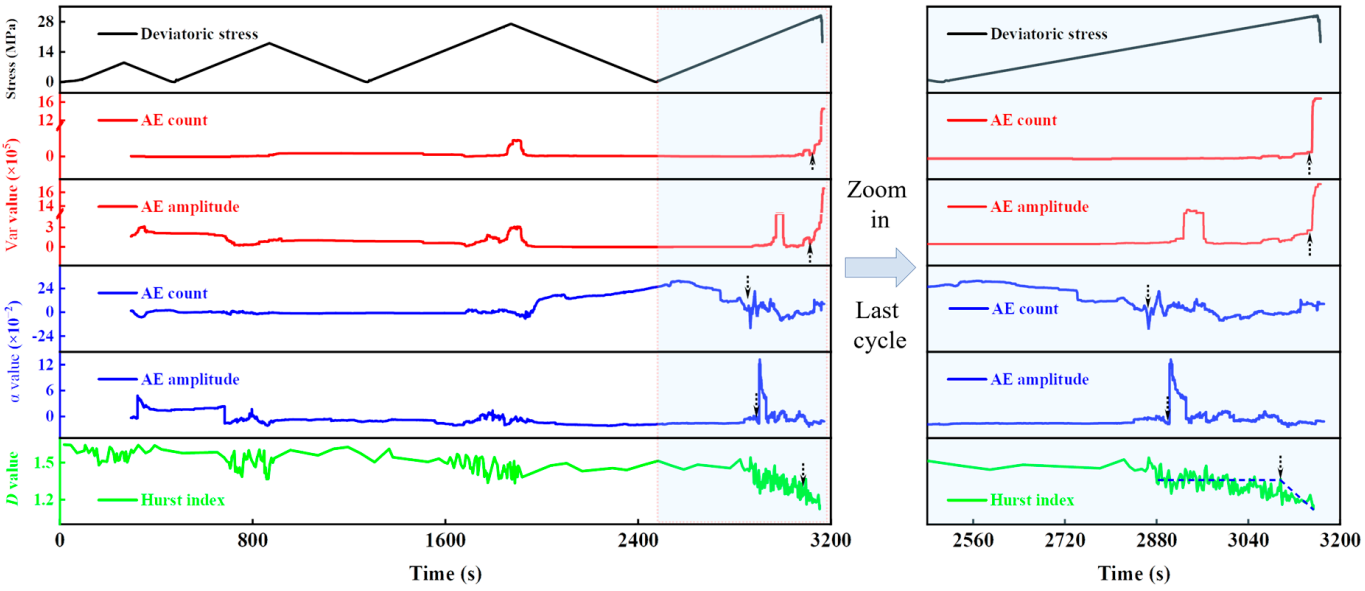

(**b**) C5-2

Figure 10. *Cont.*

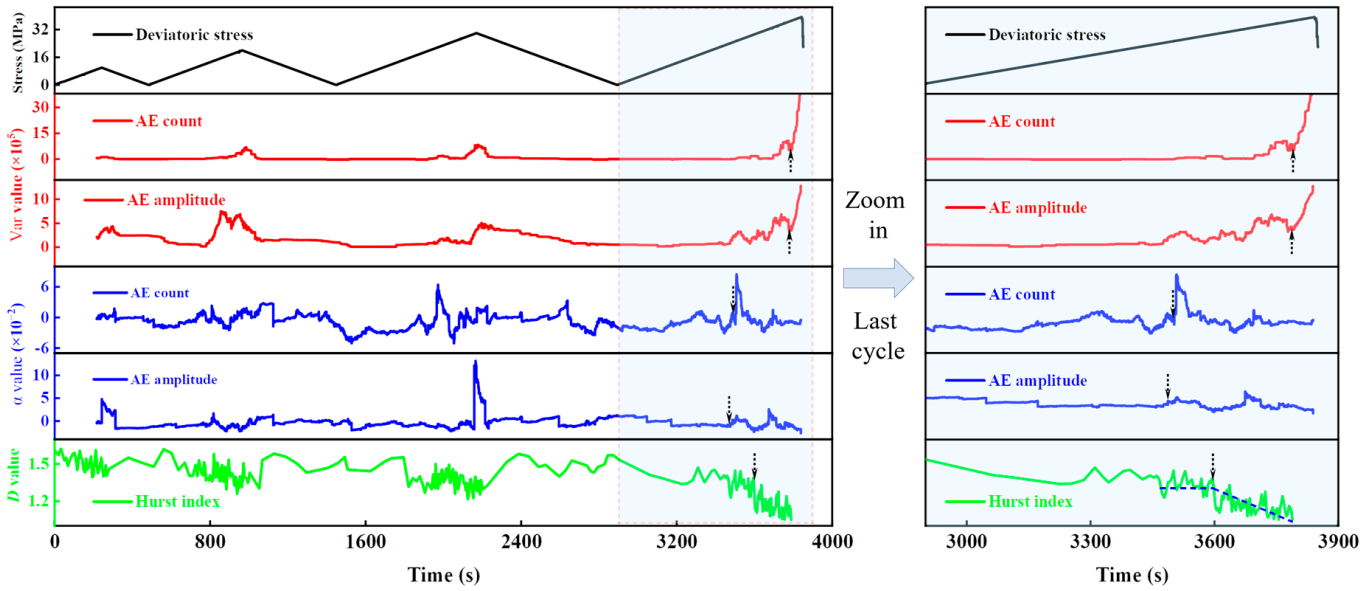

(**c**) C10-2

Figure 10. AE multi-parameter precursor response characteristics.

Before the coal sample is destroyed, the autocorrelation coefficient and variance of the two AE counts and amplitude exhibit a sudden increase. Additionally, the variance undergoes a more pronounced change at the inflection point of the mutation. Analysis from Section 4.3 demonstrates a consistent decrease in the *D* value throughout the entire loading and unloading process. Furthermore, when combined with Figure 10, it can be observed that the amplitude of the decrease significantly intensifies as the coal sample approaches destruction. Comparing the occurrence time of precursor signals under three different confining pressures, it is evident that in the presence of constricting pressure, the occurrence time of precursor signals indicating coal sample failure is advanced for several parameters. Specifically, the autocorrelation coefficient exhibits the earliest change, followed by the *D* value, while the variance change occurs last. By analyzing the changes in these three signals, the occurrence of coal sample failure can be more accurately predicted.

Coal, being a heterogeneous material, contains internal microcracks that exhibit anisotropic behavior [41]. Consequently, accurately understanding the characteristics and precision of stress damage-related early warnings becomes challenging. This study aims to address this issue by analyzing the precursory response characteristics of various parameters. The findings indicate that during multiaxial cyclic loads, the self-correlation coefficient, and variance of AE count and amplitude increase before the instability and failure of coal samples, while the *D* value decreases. These parameters exhibit timely changes in failure precursors, with increasing amplitude being particularly noteworthy. The autocorrelation coefficient of AE count and amplitude shows critical slowing down, serving as an initial signal, while the fractal dimension *D* acts as a medium-term signal. The variance in the AE count and amplitude exhibits critical slowing down and can be utilized as a critical signal. By monitoring these parameter changes, the instability and failure of coal samples can be accurately predicted, offering a reliable foundation for project monitoring and early warning. Thus, the significance of this research cannot be overstated.

6. Conclusions

To promote safety and sustainable development during deep coal mining, the mechanical and precursory varying characteristics of coalburst subjected to in-site mining cyclic loads are analyzed, and the influence of confining pressure is discussed. The AE precursor

for coal instability is identified using Hurst fractal and critical slowing down analysis. The main conclusions of this study are as follows:

The mechanical parameters, including peak stress, strain, and elastic modulus of coal samples, demonstrate an increase with increasing loading cycles. These parameters also exhibit a positive correlation with the applied confining pressure. Moreover, an examination of the energy evolution mechanism highlights that an increase in confining pressure leads to higher elastic strain energy and dissipation energy in coal samples, resulting in a gradual increase in their plasticity.

The AE count and accumulated energy show a notable correlation with cyclic stress. As the cyclic number increases, the Felicity ratio of the AE gradually decreases. Similarly, the variation in the AE RA/AF value demonstrates that with increasing stress and confining pressure, the prevalence of shear cracks rises gradually. This trend signifies the shift from tension-shear mixed-mode fracture under low confining pressure to predominantly shear fracture under high confining pressure. Furthermore, the AE responses conform to the Hurst statistical law, with increased confining pressure enhancing the predictability of deformation and failure in coal.

The abrupt escalation in the variance and autocorrelation coefficient of the AE count and amplitude, along with the reduction in the fractal D value, serve as precursory signals of impending catastrophic failure. These precursory phenomena can be categorized into early, intermediate, and imminent warning signals based on their occurrence time. These experimental findings offer significant insights that can form the basis for the development of early warning systems to mitigate coalburst disasters. By leveraging these insights, the safety and sustainability of deep coal mining operations can be greatly enhanced.

Author Contributions: X.W.: Methodology, Formal analysis, Writing—original draft, Funding acquisition. J.W.: Conceptualization, Resources, Visualization. X.Z.: Project administration, Supervision. X.L.: Validation, Data curation. S.L.: Validation, Data curation. All authors have read and agreed to the published version of the manuscript.

Funding: This research was funded by the National Key R&D Program of China (2023YFE0120500), the National Natural Science Foundation of China (Grant No. 52204249 and 52227901), the independent research project of State Key Laboratory for Fine Exploration and Intelligent Development of Coal Resources, CUMT (SKLCRSM23X005).

Institutional Review Board Statement: Not applicable.

Informed Consent Statement: Not applicable.

Data Availability Statement: Data are contained within the article.

Conflicts of Interest: The authors declare that there are no conflicts of interest.

References

1. Bukowska, M. Post-Critical Mechanical Properties of Sedimentary Rocks in the Upper Silesian Coal Basin (Poland). *Arch. Min. Sci.* **2015**, *60*, 517–534. [CrossRef]
2. Wu, L.; Wang, Z.; Ma, D.; Zhang, J.; Wu, G.; Wen, S.; Zha, Z.; Wu, L. A Continuous Damage Statistical Constitutive Model for Sandstone and Mudstone Based on Triaxial Compression Tests. *Rock Mech. Rock Eng.* **2022**, *55*, 4963–4978. [CrossRef]
3. Chen, X.; Li, L.; Wang, L. The Mechanical Effect of Typical Dynamic Disaster Evolution and Occurrence in Coal Mines. *Energy Sources Part A Recovery Util. Environ. Eff.* **2022**, *44*, 2839–2850. [CrossRef]
4. Zhou, B.; Xu, J.; Peng, S.; Yan, F.; Gao, Y.; Li, Q.; Cheng, L. Effects of Geo-Stress on the Dynamic Response of Multi-Physical Field Parameters during Coal and Gas Outbursts under True Triaxial Stress. *Int. J. Rock Mech. Min. Sci.* **2021**, *142*, 104759. [CrossRef]
5. Wang, H.; Li, J. Mechanical Behavior Evolution and Damage Characterization of Coal under Different Cyclic Engineering Loading. *Geofluids* **2020**, *2020*, e8812188. [CrossRef]
6. Chen, Y.; Lu, A.; Mao, X.; Li, M.; Zhang, L. Nonlinear Dynamics Mechanism of Rock Burst Induced by the Instability of the Layer-Crack Plate Structure in the Coal Wall in Deep Coal Mining. *Shock Vib.* **2017**, *2017*, e4051967. [CrossRef]
7. Pan, Y.; Song, Y.; Liu, J. Pattern, change and New Situation of Coal Mine Rockburst Prevention and Control in China. *Yanshilixue Yu Gongcheng Xuebao/Chin. J. Rock Mech. Eng.* **2023**, *42*, 2081–2095. [CrossRef]
8. Zhang, Y.; Yang, Y.; Ma, D. Mechanical Characteristics of Coal Samples under Triaxial Unloading Pressure with Different Test Paths. *Shock Vib.* **2020**, *2020*, e8870821. [CrossRef]

9. Li, X.; Li, H.; Yang, Z.; Sun, Z.; Zhuang, J.; Song, C.; Wang, X. Experimental Study on Triaxial Unloading Failure of Deep Composite Coal-Rock. *Adv. Civ. Eng.* **2021**, *2021*, e6687051. [CrossRef]
10. Zhou, X.; Liu, X.; Wang, X.; Xie, H.; Du, P. Failure Characteristics and Mechanism of Coal under the Coupling between Different Confining Pressures and Disturbance Loading. *Bull. Eng. Geol. Environ.* **2023**, *82*, 442. [CrossRef]
11. Li, T.; Yue, Z.; Li, J.; Chen, G.; Li, Q.; Lu, Y. Effect of Confining Pressure Strength on the Characteristics of Energy Evolution and Fatigue Fracture of the Coal-Rock Structural Body. *Fatigue Fract. Mater. Struct.* **2024**, *47*, 709–727. [CrossRef]
12. Du, X.; Xue, J.; Shi, Y.; Cao, C.-R.; Shu, C.-M.; Li, K.; Ma, Q.; Zhan, K.; Chen, Z.; Wang, S. Triaxial Mechanical Behaviour and Energy Conversion Characteristics of Deep Coal Bodies under Confining Pressure. *Energy* **2023**, *266*, 126443. [CrossRef]
13. Duan, M.; Jiang, C.; Yin, W.; Yang, K.; Li, J.; Liu, Q. Experimental Study on Mechanical and Damage Characteristics of Coal under True Triaxial Cyclic Disturbance. *Eng. Geol.* **2021**, *295*. [CrossRef]
14. Shkuratnik, V.L.; Filimonov, Y.L.; Kuchurin, S.V. Regularities of Acoustic Emission in Coal Samples under Triaxial Compression. *J. Min. Sci.* **2005**, *41*, 44–52. [CrossRef]
15. Wang, X.; Wang, E.; Liu, X.; Zhou, X. Micromechanisms of Coal Fracture: Insights from Quantitative AE Technique. *Theor. Appl. Fract. Mech.* **2021**, *114*, 103000. [CrossRef]
16. Wu, L.; Ma, D.; Wang, Z.; Zhang, J.; Zhang, B.; Li, J.; Liao, J.; Tong, J. A Deep CNN-Based Constitutive Model for Describing of Statics Characteristics of Rock Materials. *Eng. Fract. Mech.* **2023**, *279*, 109054. [CrossRef]
17. Li, D.; Wang, E.; Kong, X.; Wang, X.; Zhang, C.; Jia, H.; Wang, H.; Qian, J. Fractal Characteristics of Acoustic Emissions from Coal under Multi-Stage True-Triaxial Compression. *J. Geophys. Eng.* **2018**, *15*, 2021–2032. [CrossRef]
18. Kong, X.; Zhan, M.; Cai, Y.; Ji, P.; He, D.; Zhao, T.; Hu, J.; Lin, X. Precursor Signal Identification and Acoustic Emission Characteristics of Coal Fracture Process Subjected to Uniaxial Loading. *Sustainability* **2023**, *15*, 11581. [CrossRef]
19. Zhou, X.; Liu, X.; Wang, X.; Liu, Y.; Xie, H.; Du, P. Acoustic Emission Characteristics of Coal Failure Under Triaxial Loading and Unloading Disturbance. *Rock Mech. Rock Eng.* **2023**, *56*, 1043–1061. [CrossRef]
20. Wang, M.; Zhang, J.; Jia, B.; Du, W.; Chen, Z.; Liu, S. Research on Prediction of Coal Sample Deformation Based on Acoustic-Emission Sensitive Index. *Sustainability* **2022**, *14*, 14875. [CrossRef]
21. Shan, P.; Li, W.; Lai, X.; Zhang, S.; Chen, X.; Wu, X. Research on the Response Mechanism of Coal Rock Mass under Stress and Pressure. *Materials* **2023**, *16*, 3235. [CrossRef] [PubMed]
22. Yang, Y.; Zhang, Y.; Zhang, T. The Establishment of Segmented Constitutive Relationship of Coal under Triaxial Compression: Take the No. 3 Coal of Xinhe Colliery as an Example. *Adv. Civ. Eng.* **2020**, *2020*, e8861936. [CrossRef]
23. Wang, X.; Zhao, Y.; Gao, Y.; Sun, Z.; Liu, B.; Jiang, Y. Energy Evolution of Anthracite Considering Anisotropy Under High Confining Pressure: An Experimental Investigation. *Rock Mech. Rock Eng.* **2023**, *56*, 6735–6759. [CrossRef]
24. Gong, F.; Wang, Y. A New Rock Brittleness Index Based on the Peak Elastic Strain Energy Consumption Ratio. *Rock Mech. Rock Eng.* **2022**, *55*, 1571–1582. [CrossRef]
25. Gao, D.; Sang, S.; Liu, S.; Wu, J.; Geng, J.; Tao, W.; Sun, T. Experimental Study on the Deformation Behaviour, Energy Evolution Law and Failure Mechanism of Tectonic Coal Subjected to Cyclic Loads. *Int. J. Min. Sci. Technol.* **2022**, *32*, 1301–1313. [CrossRef]
26. Duan, H.; Ma, D. Acoustic Emission Simulation on Coal Specimen Subjected to Cyclic Loading. *Adv. Civ. Eng.* **2020**, *2020*, e3798292. [CrossRef]
27. Moradian, Z.; Einstein, H.H.; Ballivy, G. Detection of Cracking Levels in Brittle Rocks by Parametric Analysis of the Acoustic Emission Signals. *Rock Mech. Rock Eng.* **2016**, *49*, 785–800. [CrossRef]
28. Shkuratnik, V.L.; Filimonov, Y.L.; Kuchurin, S.V. Features of the Kaiser Effect in Coal Specimens at Different Stages of the Triaxial Axisymmetric Deformation. *J. Min. Sci.* **2007**, *43*, 1–7. [CrossRef]
29. Sellers, E.J.; Kataka, M.O.; Linzer, L.M. Source Parameters of Acoustic Emission Events and Scaling with Mining-Induced Seismicity. *J. Geophys. Res. Solid Earth* **2003**, *108*. [CrossRef]
30. Zhang, A.; Feng, T.; Jiang, L.; Wang, D.; Wang, Z.; Zhang, R.; Feng, G.; Zhang, Z.; Deng, J.; Ren, L. Energy Characteristics and Micro-Cracking Behaviors of Deep Slate Rock under Triaxial Loadings. *Acta Geophys.* **2022**, *70*, 1457–1472. [CrossRef]
31. Ju, S.; Li, D.; Jia, J. Machine-learning-based Methods for Crack Classification Using Acoustic Emission Technique. *Mech. Syst. Signal Process.* **2022**, *178*, 109253. [CrossRef]
32. He, M.C.; Miao, J.L.; Feng, J.L. Rock Burst Process of Limestone and Its Acoustic Emission Characteristics under True-Triaxial Unloading Conditions. *Int. J. Rock Mech. Min. Sci.* **2010**, *47*, 286–298. [CrossRef]
33. Petružálek, M.; Jechumtálová, Z.; Šílený, J.; Kolář, P.; Svitek, T.; Lokajíček, T.; Turková, I.; Kotrlý, M.; Onysko, R. Application of the Shear-Tensile Source Model to Acoustic Emissions in Westerly Granite. *Int. J. Rock Mech. Min. Sci.* **2020**, *128*, 104246. [CrossRef]
34. Rodríguez, P.; Celestino, T.B. Application of Acoustic Emission Monitoring and Signal Analysis to the Qualitative and Quantitative Characterization of the Fracturing Process in Rocks. *Eng. Fract. Mech.* **2019**, *210*, 54–69. [CrossRef]
35. Ohtsu, M. Quantitative AE Techniques Standardized for Concrete Structures. *Adv. Mater. Res.* **2006**, *13–14*, 183–192. [CrossRef]
36. Ma, T.; Ma, D.; Yang, Y. Fractal Characteristics of Coal and Sandstone Failure under Different Unloading Confining Pressure Tests. *Adv. Mater. Sci. Eng.* **2020**, *2020*, e2185492. [CrossRef]
37. Kong, X.; Wang, E.; Hu, S.; Shen, R.; Li, X.; Zhan, T. Fractal Characteristics and Acoustic Emission of Coal Containing Methane in Triaxial Compression Failure. *J. Appl. Geophys.* **2016**, *124*, 139–147. [CrossRef]
38. Biancolini, M.E.; Brutti, C.; Paparo, G.; Zanini, A. Fatigue Cracks Nucleation on Steel, Acoustic Emission and Fractal Analysis. *Int. J. Fatigue* **2006**, *28*, 1820–1825. [CrossRef]

39. Zhang, E.; Zhou, B.; Li, P. Comparative Research on the Precursory Characteristics of Critical Slowing down before the Failure of Raw Coal and Briquettes. *Bull. Eng. Geol. Environ.* **2023**, *82*, 358. [CrossRef]
40. Hao, T.; Li, F.; Tang, Y.; Zhao, L.; Wang, Z. Infrared Precursor of Pre-Cracked Coal Failure Based on Critical Slowing Down. *Geomat. Nat. Hazards Risk* **2022**, *13*, 1682–1699. [CrossRef]
41. Liu, Y.; Yin, G.; Li, M.; Zhang, D.; Huang, G.; Liu, P.; Liu, C.; Zhao, H.; Yu, B. Mechanical Properties and Failure Behavior of Dry and Water-Saturated Anisotropic Coal Under True-Triaxial Loading Conditions. *Rock Mech. Rock Eng.* **2020**, *53*, 4799–4818. [CrossRef]